The Effect of Wall Suction on the Efficiency of Transpiration Cooling in Hypersonic Boundary Layer Flow

NAYAK, Raahil, POTTS, Jonathan <http://orcid.org/0000-0001-8192-0295> and CERMINARA, Adriano

Effect of Wall Suction on Transpiration Cooling and Receptivity in Hypersonic Boundary Layer Flow

Raahil Nayak*, Jonathan Potts† and Adriano Cerminara‡
Sheffield Hallam University, Sheffield, South Yorkshire, S1 1WB, United Kingdom

Aerodynamic heating and early transition remain critical concerns in hypersonic boundary layer flows. While transpiration cooling offers effective thermal protection by introducing coolant through a porous wall, it can also enhance flow instabilities, particularly at higher blowing ratios. This study uses Direct Numerical Simulations of a Mach 7.7 flow over a flat plate to examine how coolant injection and suction influence boundary layer receptivity and disturbance growth. By introducing controlled disturbances downstream of the injection zone, the analysis tracks the evolution of generalized inflection points (GIPs) and wall pressure fluctuations. The effect of the combined use of blowing for cooling and suction on the receptivity and thermal performance of transpiration cooling is analyzed through the streamwise evolution of the disturbance modes and the distribution of cooling effectiveness on the surface. Results show that coolant injection can promote the downstream growth of instabilities at specified spanwise wavenumbers; however, the simultaneous application of suction patches appears to damp these modes in the cases with coolant injection. Moreover, while suction has been observed to reduce wall cooling performance locally near the suction region, shifting the suction patch to an upstream location appears to lead to a better recovery of the cooling effectiveness further downstream.

I. Nomenclature

F	=	Blowing Ratio
U_∞	=	Freestream Velocity
S	=	Suction Ratio
ρ	=	Density
t	=	Time
R_e	=	Reynolds Number
τ	=	Viscous Shear Stress
Pr	=	Prandtl Number
u	=	Streamwise Velocity
v	=	Wall Normal Velocity
w	=	Spanwise Velocity
x	=	Streamwise Direction
y	=	Wall Normal Direction
z	=	Spanwise Direction
M	=	Mach Number
T	=	Temperature
P	=	Pressure
e	=	Specific Total Energy
Y	=	Coolant Mass Fraction
μ	=	Dynamic Viscosity
Sc	=	Schmidt Number
D	=	Diameter of Pore

*PhD Researcher, School of Engineering and Built Environment
†Senior Lecturer, School of Engineering and Built Environment
‡Senior Lecturer, School of Engineering and Built Environment MAIAA

Δ_x = Spacing in streamwise direction
Δ_y = Spacing in wall normal direction
Δ_z = Spacing in spanwise direction

II. Introduction

The development of high-speed transportation systems, especially in the context of hypersonic vehicles and space reentry platforms, continues to gain momentum in the aerospace sector. However, operating in such extreme regimes introduces significant challenges, particularly due to intense aerodynamic heating and the resulting compromised structural integrity of the vehicle. This aerodynamic heating occurs due to the dissipation of a huge amount of kinetic energy into thermal energy as a result of (i) the shock wave in front of the leading edge and (ii) viscous effects within the boundary layer[1]. To counteract these effects, various film-cooling techniques have been explored to provide thermal protection by introducing a cooler fluid into the boundary layer[2–7]. Two common strategies have emerged: effusion cooling, which injects coolant through discrete jets or slots, and transpiration cooling, which relies on a porous surface to deliver a more uniform coolant distribution. While transpiration cooling generally forms a more consistent coolant layer, effusion cooling with two-dimensional slot configurations has demonstrated advantages in delaying transition by suppressing certain three-dimensional effects[8, 9].

Transition in compressible boundary layers has been widely studied through both experiments and numerical simulations, particularly with respect to the instability modes responsible for transition. In low Mach number regimes, Saric et al[10] showed that receptivity is largely governed by interactions between freestream acoustic or vortical disturbances and surface imperfections, such as roughness or waviness, which efficiently generate TS waves at the leading edge, highlighting the critical role of surface features in the early stages of boundary-layer instability. Meanwhile, at higher Mach numbers, and especially in hypersonic flows, second-mode or Mack-mode instabilities dominate, leading to rapid amplification and transition[11]. Balakumar[12] studied a Mach 3.5 flow over a flat plate and identified short-wavelength slow waves, linked to vorticity and entropy fluctuations, as key contributors to the growth of TS-like instabilities. The receptivity of hypersonic boundary layers has received growing attention in recent years. Ma et al[13] studied a Mach 4.5 flow over a flat plate and demonstrated that stable wave modes (denoted Mode I and II) play a crucial intermediary role through resonance with freestream acoustic waves in exciting the unstable second mode. Their direct numerical simulations and linear stability analysis elucidated how wall perturbations can trigger amplification of these second-mode instabilities in flat-plate hypersonic flow, providing a relevant foundation for receptivity analysis in similar configurations. Research by Hader et al[14] further demonstrated that second-mode instabilities are highly responsive to entropy-layer distortions. Fedorov et al[15] showed that local peaks in entropy and wall temperature gradients greatly influence the initial growth of disturbances.

An investigation into passive and active cooling approaches on leading-edge configurations was carried out by Esser et al[16], informing the structure used in later experiments by Tanno et al at JAXA[17]. Experiments conducted in a free piston shock tunnel showed that in low Reynolds number flows, the cooling effect extended over large downstream distances, largely due to the laminar state of the boundary layer, consistent with the findings of Ifti et al[4]. In contrast, high Reynolds number cases showed a sharp drop in efficiency after injection, owing to transition to turbulence and the resultant enhanced mixing within the turbulent boundary layer.

In the presence of film cooling, high blowing ratios have been found to amplify boundary layer disturbances, often triggering earlier transition and diminishing cooling effectiveness[18]. Unnikrishnan et al[19] analyzed the response of high-speed boundary layers to various types of external forcing and found that wall heating or cooling can shift the dominant instability modes, aligning with the work of Guo et al[20] and Unnikrishnan et al[21]. Theoretical and computational studies, such as those by Egorov et al[22] and Zhuang et al[23], have demonstrated that localized suction can effectively suppress both Tollmien-Schlichting and second-mode instabilities in hypersonic boundary layers.

While the overall effects of coolant injection on boundary layer stability have been explored, the specific dynamics of disturbances under the influence of injection are less understood. The present study addresses this gap by examining how different blowing ratios impact the evolution of instabilities, with a focus on generalized inflection point (GIP) dynamics and associated pressure fluctuations. By investigating how the injected coolant alters the downstream evolution of boundary layer disturbances, this study aims to better understand the mechanisms driving transition in cooled hypersonic flows. In parallel with injection-based methods, suction has been studied as a boundary layer control strategy, particularly for its stabilizing effect on convective instabilities in high-speed flows.

Suction operates by extracting low-momentum fluid from the near-wall region, thereby reducing the amplification of disturbances and delaying transition. Building on these insights, the present study explores the implementation of

discrete suction patches downstream of coolant injection regions, with the goal of mitigating the destabilizing effects introduced by blowing. By applying suction in targeted downstream zones where instabilities amplify, a combined injection - suction configuration is investigated for its potential to restore boundary layer stability. This calibrated hybrid approach seeks to harness the protective effects of blowing alongside the stabilizing benefits of suction, offering a novel framework for transition control in hypersonic boundary layers.

III. Methodology

A. Governing Equations

The system of the three-dimensional dimensionless governing equations for compressible flow, written in conservation form, under the assumption of constant specific heats, is given in Cartesian coordinates as

$$\frac{\partial \rho}{\partial t} + \frac{\partial \rho u_j}{\partial x_j} = 0 \tag{1}$$

$$\frac{\partial \rho u_i}{\partial t} + \frac{\partial \rho u_i u_j}{\partial x_j} = -\frac{\partial p}{\partial x_i} + \frac{1}{R_e}\frac{\partial \tau_{ij}}{\partial x_j} \tag{2}$$

$$\frac{\partial (\rho e)}{\partial t} + \frac{\partial \left(\rho e + \frac{p}{\rho}\right) u_j}{\partial x_j} = \frac{1}{(\gamma - 1) R_e Pr M^2}\frac{\partial}{\partial x_j}\left(\frac{\partial \mu T}{\partial x_j}\right) + \frac{1}{R_e}\frac{\partial \tau_{ij} u_i}{\partial x_j} \tag{3}$$

$$\frac{\partial \rho Y}{\partial t} + \frac{\partial}{\partial x_j}\left(\rho Y u_j - \frac{\mu}{R_e Sc}\frac{\partial Y}{\partial x_j}\right) = 0 \tag{4}$$

where (4) is the mass conservation equation for the coolant species, which is air in the considered case. The terms ρ, ρu, ρv, ρw and ρe, and ρY are the conservative variables of the system of equations, where ρ is the density, u, v and w are the velocity components respectively in the X, Y and Z directions, e is the specific total energy per unit mass and Y is the coolant mass fraction. The physical variables are normalized through their free-stream reference values, except for the pressure, which is normalized with the term $\rho^*_\infty U^2_\infty$. The superscript $*$ is used to denote dimensional values. The characteristic length chosen to normalize the length scales is the boundary-layer displacement thickness (δ^*) of the similarity solution at the inflow. The characteristic fluid dynamic time is δ^*/U^*_∞. The terms R_e, Pr, Sc, M and γ are the dimensionless parameters of the flow. The Reynolds number is defined as $R_e = (\rho^*_\infty U^*_\infty \delta^*)/\mu^*_\infty$; the Prandtl number is set to 0.72, the Schmidt number is set to 1, and γ is equal to 1.4, for air. Sutherland's law is used to model the viscosity. Thermal diffusion is neglected, as it was observed to be negligible if the species in a binary mixture have similar properties [24].

Transpiration cooling is implemented in the form of wall normal jets emerging from uniformly spaced circular pores, distributed over a given length in the streamwise direction and from end to end in the spanwise direction, to simulate the effect of a porous medium. The injection rate is modeled as a quantity called the blowing ratio which is defined in Equation 5.

$$F = (\rho v)_{coolant} / (\rho u)_{freestream} \tag{5}$$

where $(\rho v)_{coolant}$ is the momentum of the coolant at the wall and $(\rho u)_{freestream}$ is the momentum of the freestream flow. The coolant momentum is implemented in the code as a function of the streamwise (x) and spanwise (z) directions, in the form of a cubic sine function as shown in Equation 6.

$$(\rho v)_{\text{coolant}} = F \left| \sin^3\left(\frac{x}{D}\right) \sin^3\left(\frac{z}{D}\right) \right| \tag{6}$$

where D is the diameter of the pore fixed at a non-dimensional value of 1.6 and F is a measure of the intensity of injection, both values being defined in the code. The transpiration cooling model has been assessed in recent studies, which include validation against existing experimental data [8][18]. Suction of the fluid (a mixture of the coolant and boundary layer air) out of the flow is assumed to be through a porous section in the wall modelled in a manner similar to the implementation of the blowing section, shown in Equation 7, where S is the suction ratio.

$$(\rho v)_{\text{suction}} = -S \left| \sin^3\left(\frac{x}{D}\right) \sin^3\left(\frac{z}{D}\right) \right| \tag{7}$$

B. Code Used

The DNS computations in the present research utilize the SBLI (shock-boundary-layer interaction) code, developed extensively at the University of Southampton. The code employs a spatial discretization scheme based on a fourth-order central finite difference and incorporates a boundary treatment of the same order [25]. The code utilizes a Ducros sensor to preserve the rotational flow regions from the numerical dissipation of the shock-capturing scheme[26]. The latter is based on a second-order Harten-Yee TVD scheme, with a specific compression method (Harten's switch) which concentrates artificial dissipation in sharp gradient regions and minimizing dissipation in smooth regions[27]. An entropy-splitting method is applied to enhance the stability of the high-order central scheme[28].

Temporal integration is achieved using a third-order Runge-Kutta scheme. The code operates using MPI libraries and has been configured for parallel execution by dividing the domain into sub-domains, each assigned to a specific processor. Validation of the code can be found in the work of De Tullio [29], where DNS results are compared with PSE results for the case of transition induced by a discrete roughness element in a boundary layer at Mach 2.5, and Cerminara[30] for various hypersonic flow configurations.

C. Case Setup

The flow conditions for the present study, summarized in Table 1, are based on the experimental work of Tanno et al[17]. A Mach 7.7 flow over a flat plate is simulated in a computational domain extending 400 in the streamwise direction, 30 normal to the wall, and 16 in the spanwise direction, with the mesh parameters set at $\Delta_x = 0.213$, $\Delta_y = 0.149$ and $\Delta_z = 0.16$ as shown in Table 2. Transpiration cooling is modeled using wall-normal jets that emerge from uniformly spaced circular pores, distributed from $x = 5$ to $x = 30$ across the full span. To investigate the receptivity and evolution of flow instabilities, wall-based disturbances were imposed downstream between $x = 40$ and $x = 64$, with a frequency of 193 kHz. Further details on the disturbance field, including streamwise and spanwise wavenumbers corresponding to unstable mode waves, as well as imposed disturbance amplitude, can be found in the work of Cerminara et al[18]. An initial study was conducted using three different wavelengths in the spanwise direction, detailed in Table 3, where β is the integer value assigned to the spanwise modes of the disturbances induced in the flow. The results of this study are discussed in Section IV.A.

Table 1 Flow Conditions for the Present Simulation Study

Quantity	Value
Freestream Temperature	259 K
Wall Temperature	290 K
Freestream Pressure	2.382 kPa
Freestream Density	0.03131 kg/m^3
Freestream Velocity	2513.2 m/s
Unit Reynolds Number	4.75x10^6 $/m$

Table 2 Grid Setup

Parameter	Value
L_x	400
L_y	30
L_z	16
Δ_x	0.213
Δ_y	0.149
Δ_z	0.16

Table 3 Cases Studied wrt Disturbance Variation

Case ID	β	λ_z
A	4	4
B	2	8
C	1	16

The second phase of the study utilised only the oblique mode with spanwise wavelength $\lambda_z = 4$ in two cases, without blowing($F = 0$) and with blowing($F = 0.009$), which corresponds to the highest intensity of blowing tested by Cerminara et al[18]. The study is extended to the case of suction added locally, in addition to coolant injection, in order to damp the boundary-layer instabilities. In each of these cases, simulations were initially carried out without any suction introduced. Following this, a suction patch was incorporated between $x = 200$ and $x = 240$, downstream of the region where disturbances were induced. In the no blowing case, two intensities of suction were investigated, with $S = 0.0045$ and $S = 0.009$. In the cases with coolant injection at $F = 0.009$, suction was implemented at $S = 0.00225$, $S = 0.0045$, $S = 0.00675$ and $S = 0.009$, corresponding to 25%, 50%, 75% and 100% of the coolant injection intensity.

IV. Results and Discussion

A. Varying the Spanwise Wavelength of the Disturbances

In compressible hypersonic boundary layers, the emergence of instability is closely associated with the presence of generalized inflection points (GIPs) in the boundary layer[31]. These points, identified by the condition $(\rho u')' = 0$, where ρ and u denote the mean density and streamwise velocity, are the compressible-flow counterparts of classical inflection points in incompressible boundary layers. The existence of a GIP indicates that the flow is vulnerable to inviscid instability mechanisms, allowing for the amplification of discrete instability modes. Consequently, GIPs provide a valuable criterion for anticipating the onset of instability and assessing the receptivity characteristics of hypersonic boundary layers. The $(\rho u')'$ curve was plotted at different streamwise locations and GIPs were located on the curve, depicted by the black dots in Figures 1, 2 and 3 for Cases A, B and C detailed in Table 3, respectively. The number of GIPs in the boundary layer below the δ_{99} line, which signifies the height above the wall at which the streamwise velocity is approximately 99% of that of the freestream streamwise velocity, are recorded and compared. The $\lambda_z = 4$ case at $F = 0$ exhibits a distinct GIP structure, with several zero-crossing points, particularly near $x = 150$ to $x = 200$. All $F = 0.009$ cases exhibit minimal inflectional activity across the domain, with 2 GIPs observed at all streamwise locations, demonstrating stabilized flow.

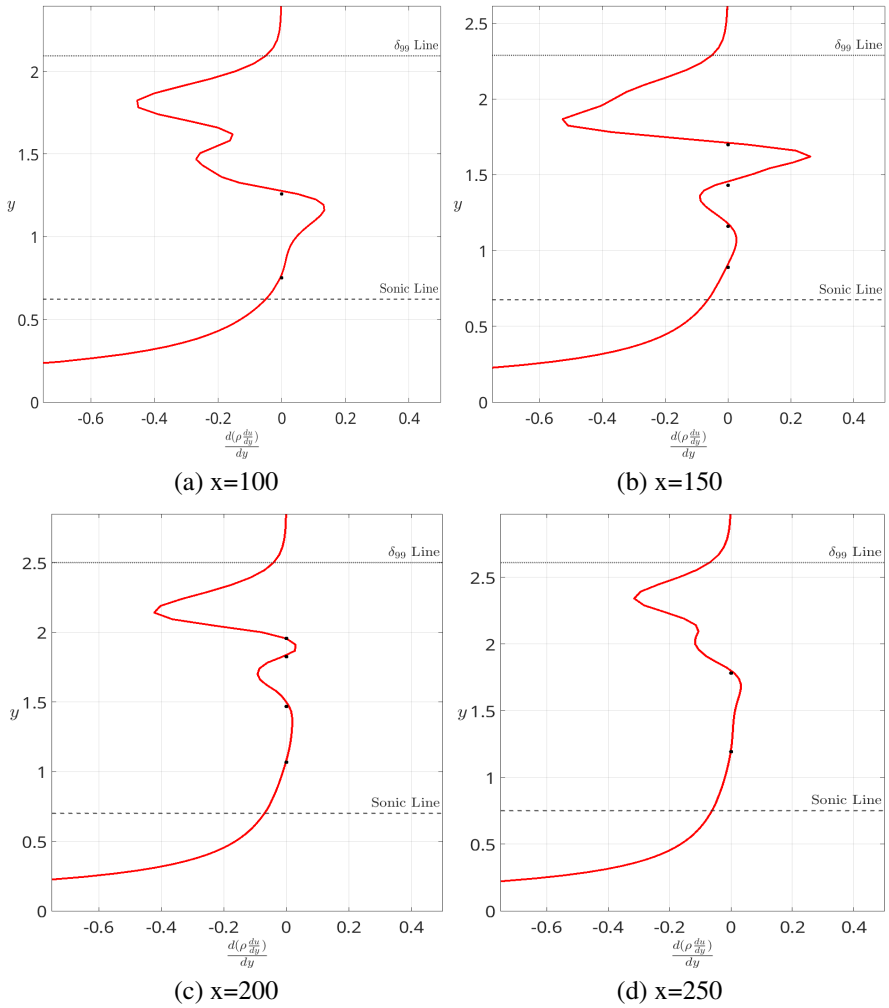

(a) x=100 (b) x=150

(c) x=200 (d) x=250

Fig. 1 $(\rho U')'$ Variation and GIP Locations for Case A F 0

The GIP profiles clearly demonstrate that the $\lambda_z = 4$ configuration exhibits four distinct zero crossings in the $(\rho U')'$ distribution across the boundary layer, marked by sharp oscillations and turning points, especially in the region between $y = 1$ and $y = 2$. This behavior is consistent at both $x = 150$ and $x = 200$, indicating a strongly inflectional boundary layer profile. In comparison, the $\lambda_z = 8$ case shows smoother profiles with only two zero crossings at each streamwise location, indicating a more stable and less inflectional character, except at $x = 150$. For the $\lambda_z = 16$ configuration, the profiles are even smoother. While four zero crossings are technically visible at $x = 150$, they are closely spaced and less pronounced. At $x = 200$, the number of zero-crossings reduces to two, resembling the behavior seen in the $\lambda_z = 8$ case. The curve is also observed to smoothen out at all locations with an increase in the wavelength of the disturbances. This trend highlights that among the three cases, the $\lambda_z = 4$ configuration consistently supports the strongest and most persistent inflectional behavior, suggesting a high susceptibility to instabilities, justifying its selection for further investigation of suction effects in Section IV.B.

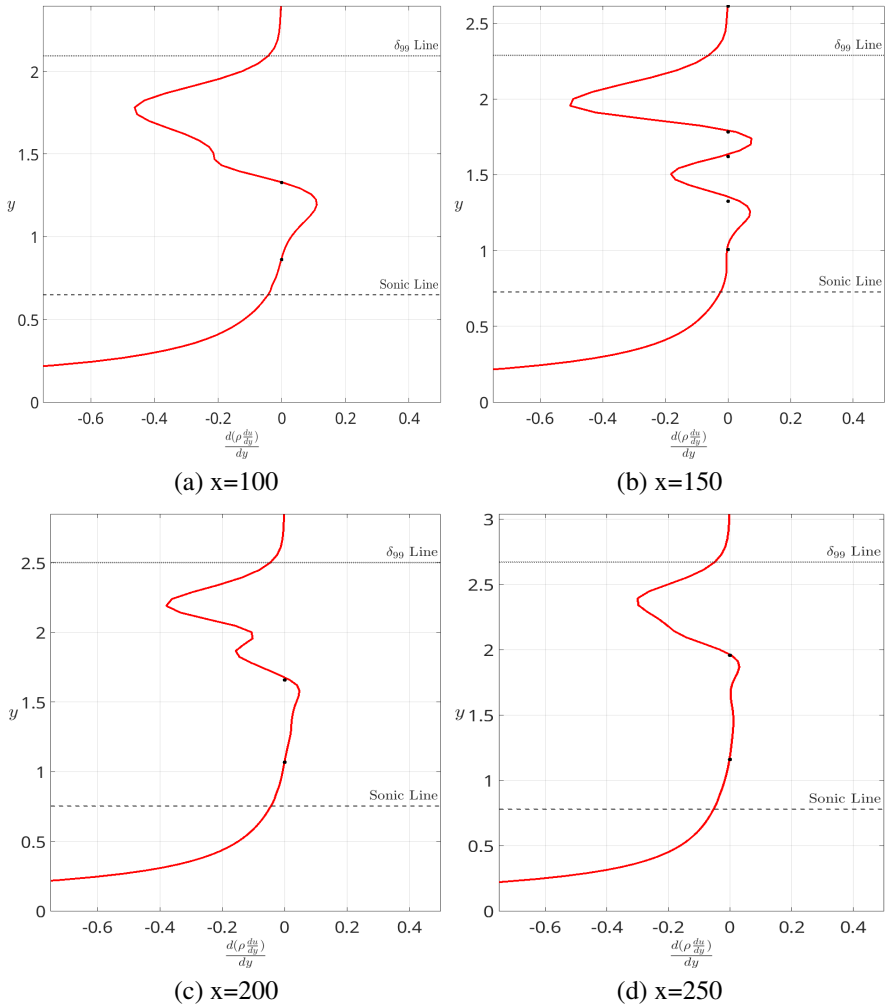

(a) x=100 (b) x=150

(c) x=200 (d) x=250

Fig. 2 $(\rho U')'$ Variation and GIP Locations for Case B F 0

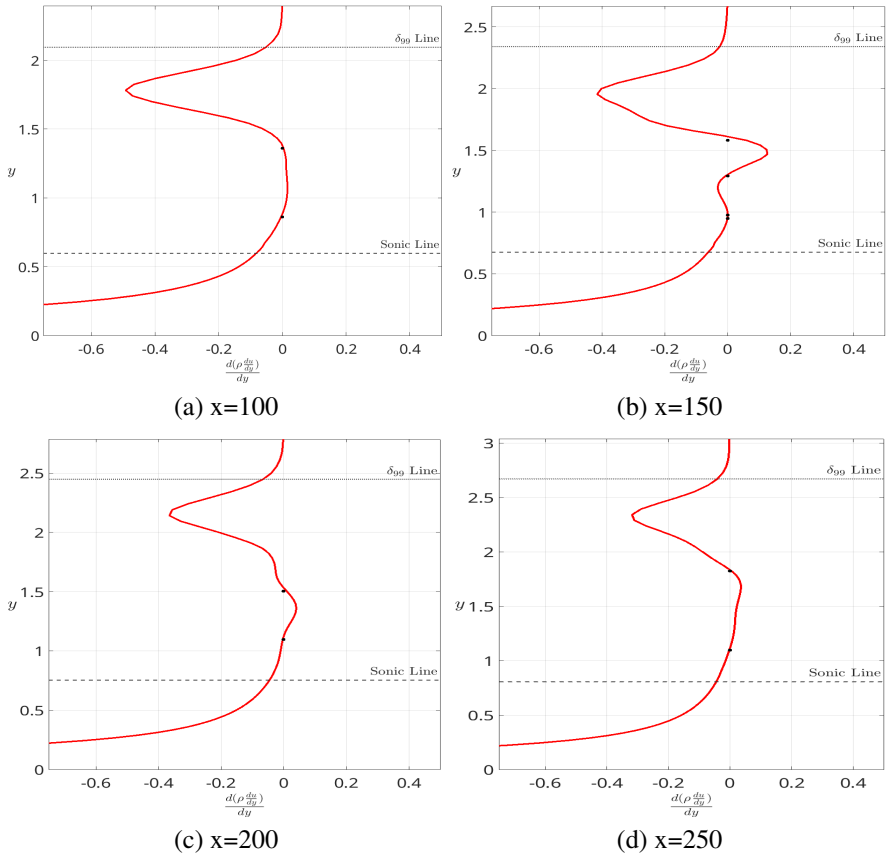

(a) x=100 (b) x=150

(c) x=200 (d) x=250

Fig. 3 $(\rho U')'$ Variation and GIP Locations for Case C F 0

B. Effect of Suction on the λ_z = 4 Case in High Blowing Case ($F = 0.009$)

Pressure fluctuation amplitudes shown in the figures in this section were obtained by performing a Fast Fourier Transform (FFT) on time-resolved wall-pressure signals along the streamwise direction. The amplitude plotted for each case corresponds to the Fourier component at the forcing frequency of 193 kHz, which alludes to the fundamental frequency of the induced disturbances. The results are presented at different spanwise wave numbers, β_0 being the 2D mode and β_1, β_2, β_3 and β_4 representing the first, second, third and fourth 3D modes, respectively.

1. Suction Effects Without Coolant Injection ($F = 0$)

Figure 4 shows the evolution of the $\beta = 0$ pressure fluctuation mode. In the baseline disturbed case without suction (red line in Figure 4), the disturbance grows sharply after the forcing region and decays smoothly beyond $x \approx 130$. When suction is applied between $x = 200$ and $x = 240$, the disturbance amplitude directly above the application point reduces slightly, following a similar profile to the case without suction until $x = 205$. However, a secondary rise in amplitude occurs downstream of the suction zone, between $x = 250$ and $x = 350$, with the peak of this rise being proportional to the strength of the suction imposed. This re-amplification suggests that suction alters the base flow, introducing 2D wave modes, which are amplified immediately downstream of the suction region, before decaying further downstream. Figures 5, 6, 7 and 8 show the streamwise behavior of the oblique modes β_1, β_2, β_3 and β_4. Similar to the 2D modes, suction appears to induce also oblique disturbances downstream (although at lower amplitudes compared to the 2D waves). High suction leads to local amplification in the β_1, β_2 and β_3 modes, rather than suppression with the β_2 mode amplifying downstream of the suction patch. For moderate suction cases, the overall amplitudes are lower, but there is still observable amplification in $\beta = 2$.

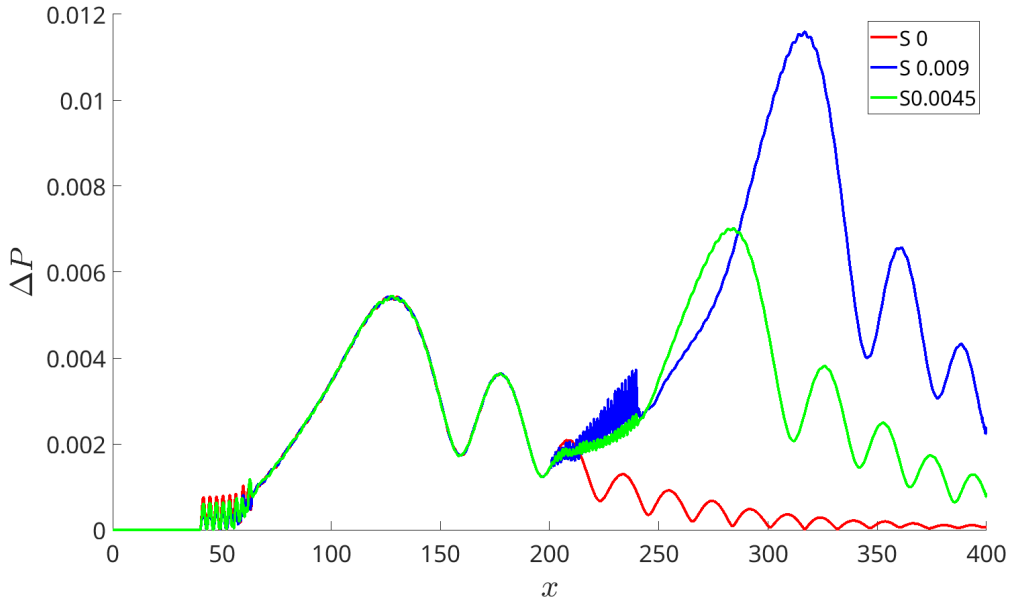

Fig. 4 Streamwise evolution of $\beta = 0$ pressure mode amplitude (F = 0)

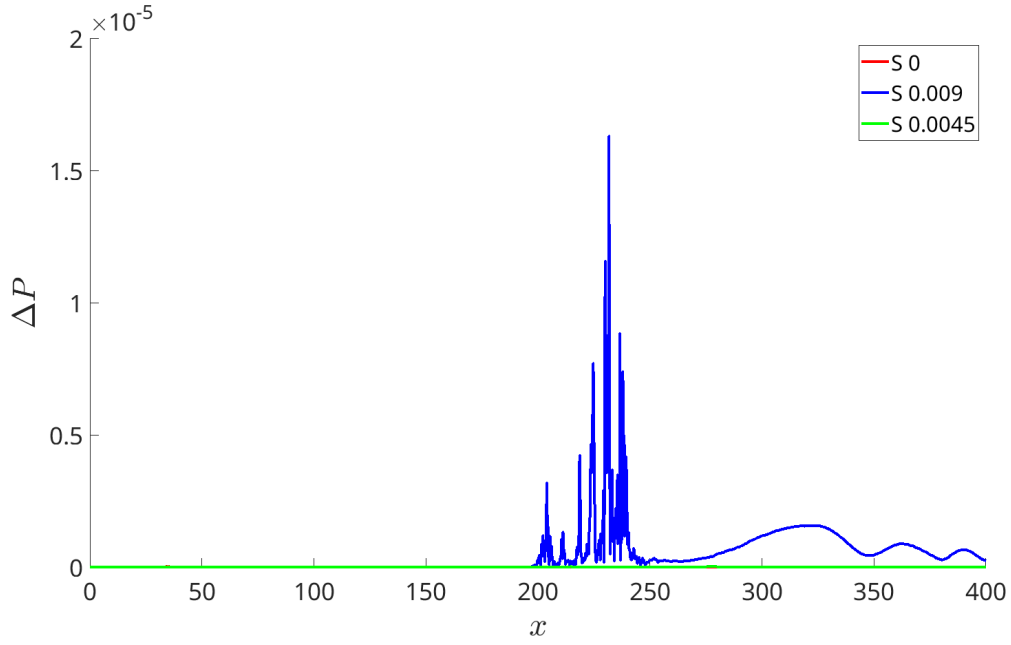

Fig. 5 Streamwise evolution of $\beta = 1$ pressure mode amplitude (F = 0)

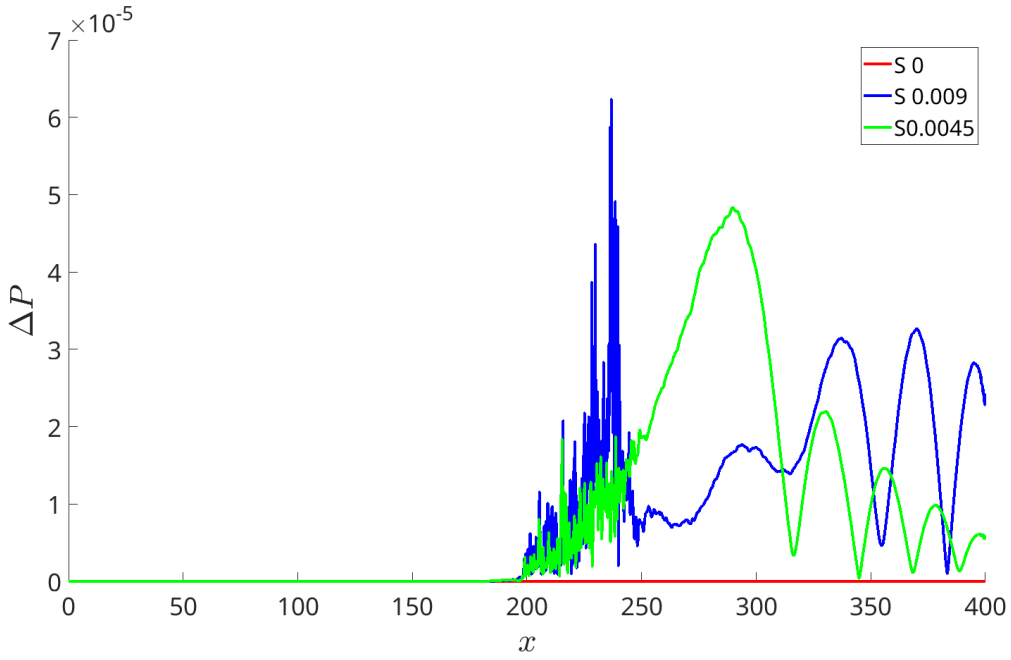

Fig. 6 Streamwise evolution of $\beta = 2$ pressure mode amplitude (F = 0)

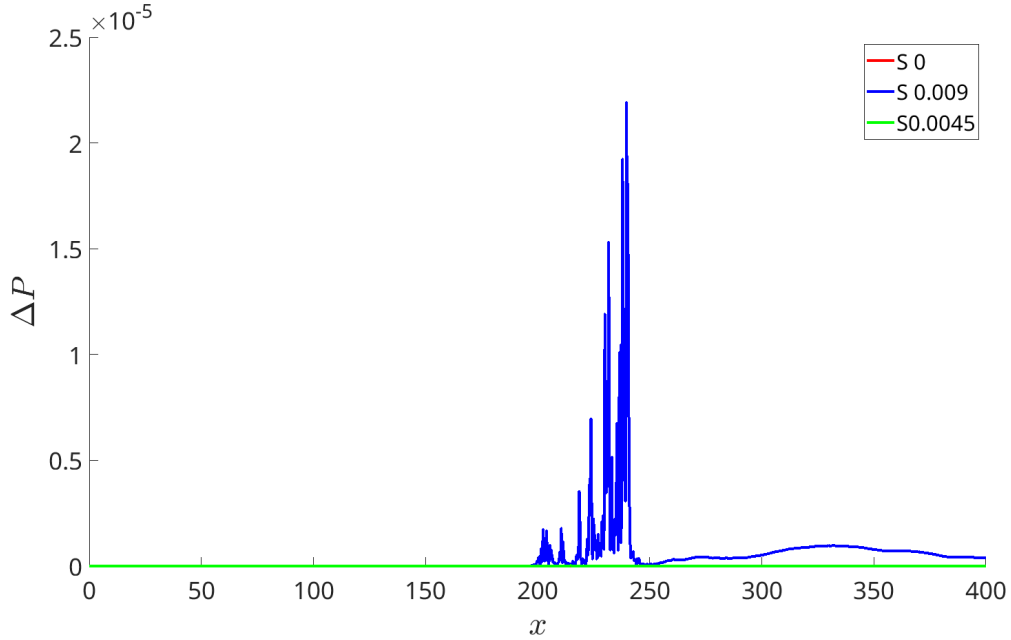

Fig. 7 Streamwise evolution of $\beta = 3$ pressure mode amplitude (F = 0)

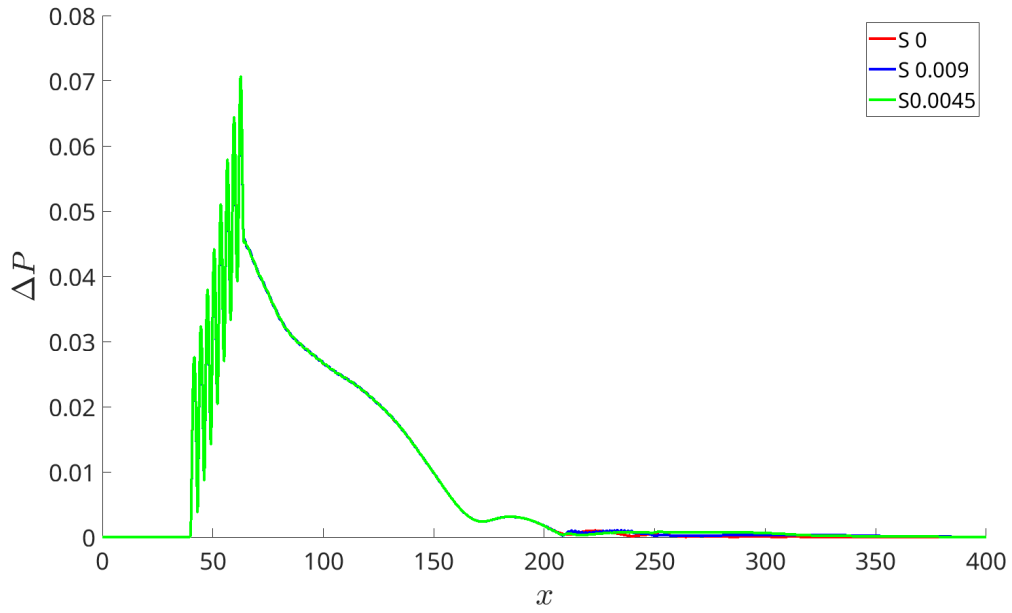

Fig. 8 Streamwise evolution of $\beta = 4$ pressure mode amplitude (F = 0)

Figure 8 shows the evolution of the fundamental forced mode, β_4. As expected, this mode dominates early in the domain due to direct forcing and decays gradually downstream. With suction, the amplitude initially remains close to the disturbed baseline but exhibits a sharper drop over the suction patch. However, for both suction strengths, there is a slight downstream rise in amplitude, between $x = 300$ and $x = 350$, reinforcing the trend seen in β_0 and β_3 curves. This indicates that suction might modify the flow topology in a way that sustains or reintroduces instability mechanisms downstream, despite reducing local energy content near the wall, which is in line with the study by Wang et al[32], which found that without proper tuning (in terms of strength and frequency), suction can enhance certain modes. Overall, these results show that in the absence of upstream blowing, suction does not always play a stabilizing role. A GIP analysis was carried out on the $F = 0$ case in order to further understand the mode behaviour. Figures 9 and 10 depict the $(\rho u')'$ curve for the cases with moderate and high suction respectively. It is clearly visible that the suction initially increases the instability of the boundary layer immediately downstream of the suction patch at $x = 250$, where four GIPs can be seen in the moderate suction case. However, the number of zero-crossing points reduces with an increase in the strength of the suction. Figures 10b and 10c show 0 GIPs in the boundary layer, which suggest a more stable behaviour than the base flow case seen in Figure 1.

The disappearance of GIPs in the high suction case and the smoothening of the $(\rho u')'$ curve in the moderate suction case indicate a significant suppression of inflectional behaviour, which is consistent with the studies using suction as a flow control mechanism[23, 33]. However, the accompanying downstream disturbance resurgence in some modes hints at the emergence of alternative: non-inflectional behaviour, possibly due to viscous instabilities, or residual receptivity effects driven by suction-induced flow restructuring, which essentially shifts the instability regions downstream[33].

Figure 11 depicts the pressure fluctuation amplitude contours over the wall in the streamwise and spanwise direction. Figure 11a shows strong streaks between $x = 50$ and $x = 120$, immediately downstream of the section where disturbances are induced, indicative of strong 3D modes. These disturbances completely dissipate into the flow near $x = 200$ with the downstream flow relatively unperturbed. Figures 11b and 11c show a similar trend as seen in Figure 11a. However, Figure 11b also presents with a relatively weak 2D wavefront further downstream between $x = 250$ and $x = 300$ and another much weaker and narrower (in the streamwise direction) 2D wavefront appearing further downstream. In Figure 11c, these 2D wavefronts appear to grow stronger in amplitude. These 2D wavefronts appear to mix with weak 3D modes, especially between $x = 300$ and $x = 350$. In summary, while suction proves effective at eliminating the inflectional inviscid instabilities, it may also introduce new spatial complexity that sustains or redistributes instability further downstream when there is no coolant injection upstream. This response highlights the need for carefully tuned suction parameters to achieve effective flow control in high-speed boundary layers.

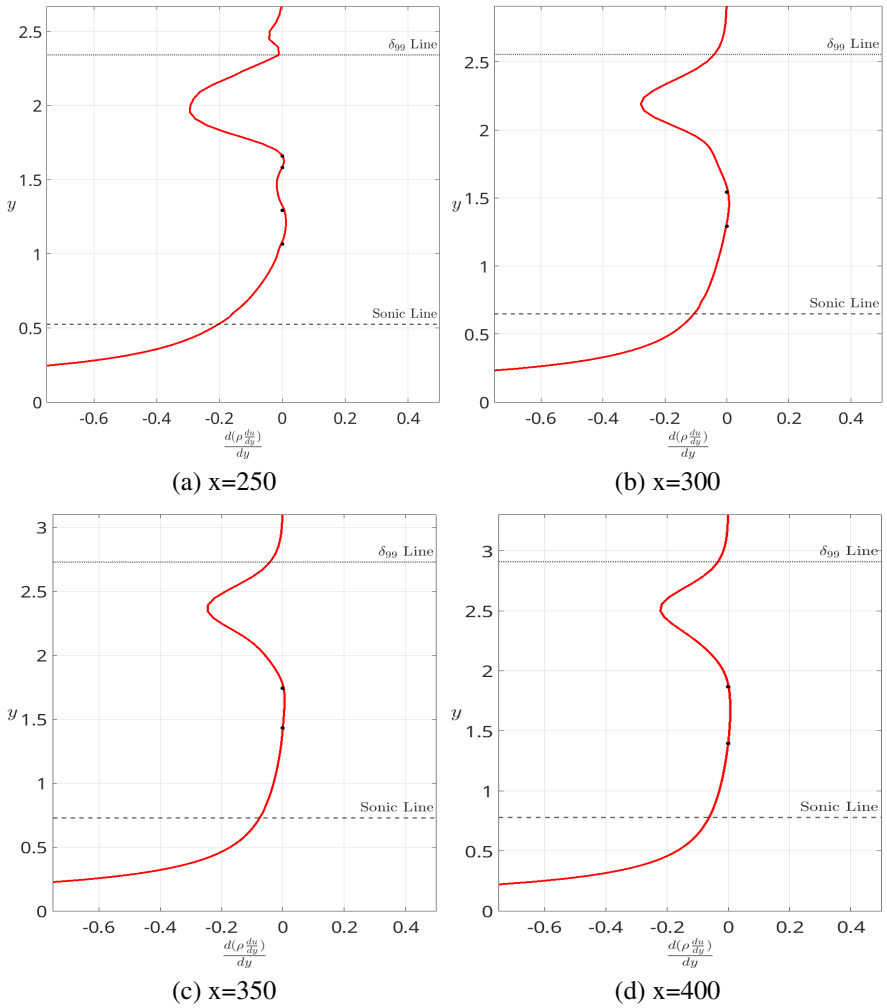

(a) x=250 (b) x=300

(c) x=350 (d) x=400

Fig. 9 $(\rho U')'$ Variation and GIP Locations for F=0 S=0.0045

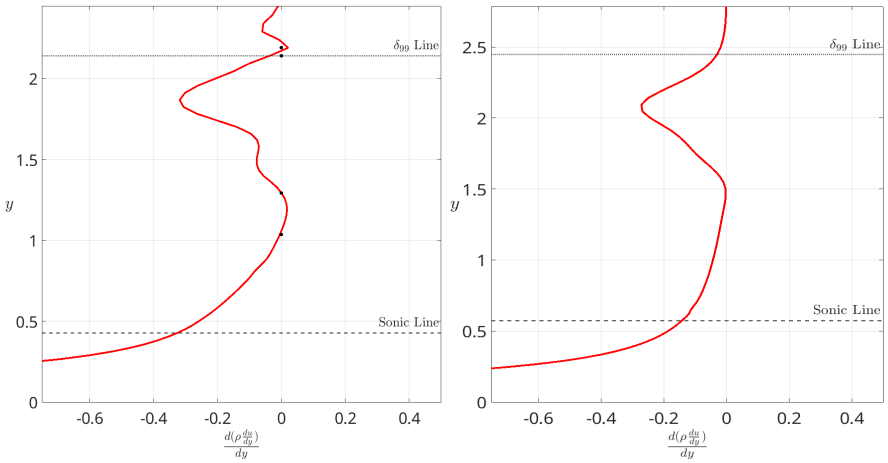

(a) x=250 (b) x=300

(c) x=350 (d) x=400

Fig. 10 $(\rho U')'$ Variation and GIP Locations for F=0 S=0.009

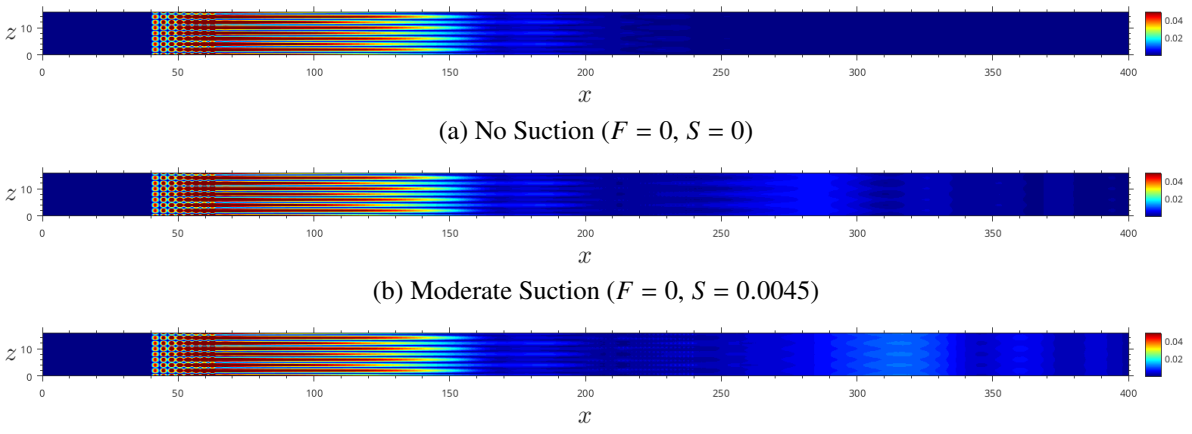

(a) No Suction ($F = 0$, $S = 0$)

(b) Moderate Suction ($F = 0$, $S = 0.0045$)

(c) High Suction ($F = 0$, $S = 0.009$)

Fig. 11 Wall pressure fluctuation contours showing spatial growth of disturbances for different suction strengths with no coolant injection ($F = 0$)

2. Suction Effects with Coolant Injection (F = 0.009)

Figures 12, 13, 14 and 15 show the evolution of modal amplitudes when suction is applied downstream of the disturbance region in the $F = 0.009$ case. The $\beta = 0$ mode (Figure 12) is damped relative to the $F = 0$ case, particularly for the moderate suction strength. However, stronger suction produces low-amplitude oscillations near the suction patch and a delayed secondary growth downstream. The 3D mode (Figures 13 also show a reduction in amplitude due to the suction patch. β_1 mode is consistently suppressed with increasing suction strength. β_2 and β_3 modes show partial suppression, though the effect of suction is not too clear since the fluctuation appears to be very random. Moving the suction patch upstream (dashed lines) does show suppression of all the β_1 and β_3 modes in the region of inducing disturbances with a slight local amplification right above and immediately downstream of the suction patch, between $x = 100$ and $x = 200$, similar to the trend observed above the suction patches downstream in the other cases. However, it is noteworthy that shifting the suction patch upstream damps all the modes further downstream, between $x = 300$ and $x = 400$, especially in case of the β_0 and β_1 modes, which are the primary drivers of instability in the Mach 7.7 boundary layer as investigated by Cerminara et al[18]. Figure 16 shows the evolution of the fundamental forced mode, β_4, in the high-blowing configuration ($F = 0.009$). The presence of disturbances due to blowing leads to the substantial attenuation of the disturbance immediately downstream of the forcing region. The addition of suction further suppresses the weak fluctuations, with higher suction ratios leading to greater decay in amplitude. These results indicate that, in the presence of coolant injection, suction is effective in damping instability modes at different spanwise wavenumbers. Placing the suction patch immediately downstream of the disturbance strip yields the strongest suppression of all instability modes.

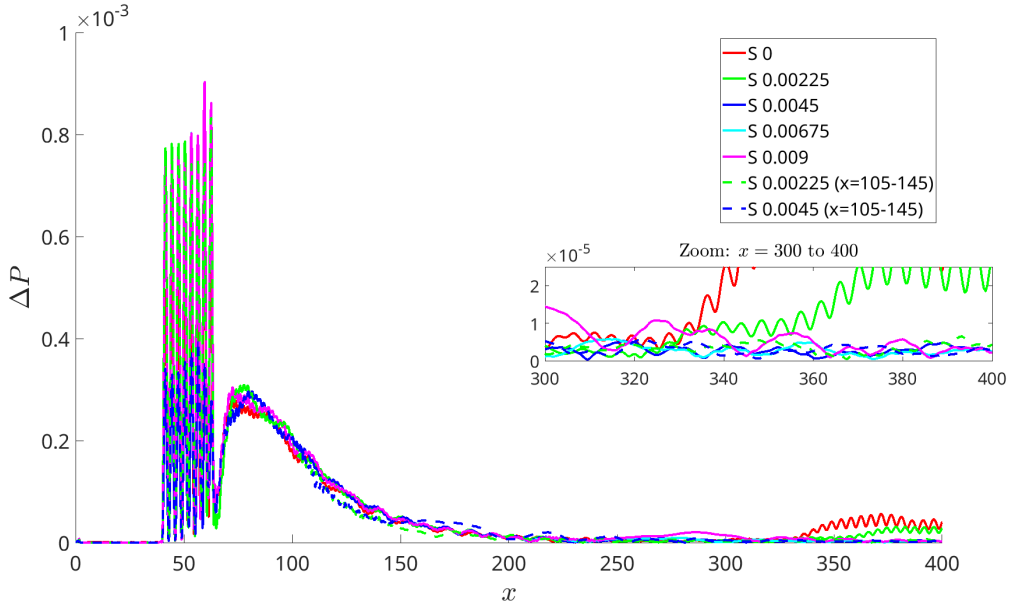

Fig. 12 Streamwise evolution of $\beta = 0$ pressure mode amplitude (F = 0.009)

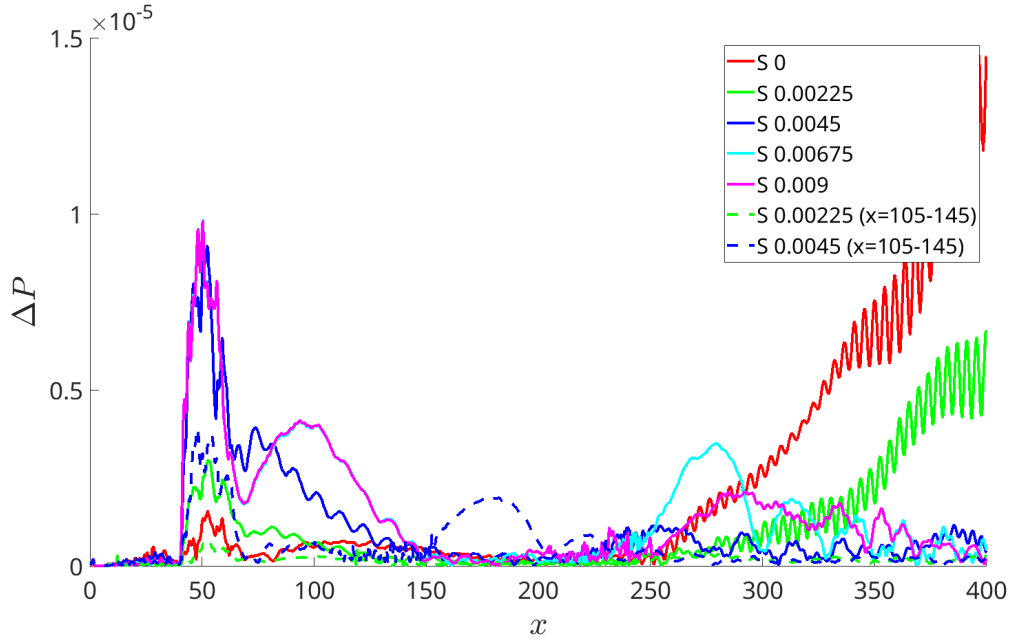

Fig. 13 Streamwise evolution of β = 1 pressure mode amplitude (F = 0.009)

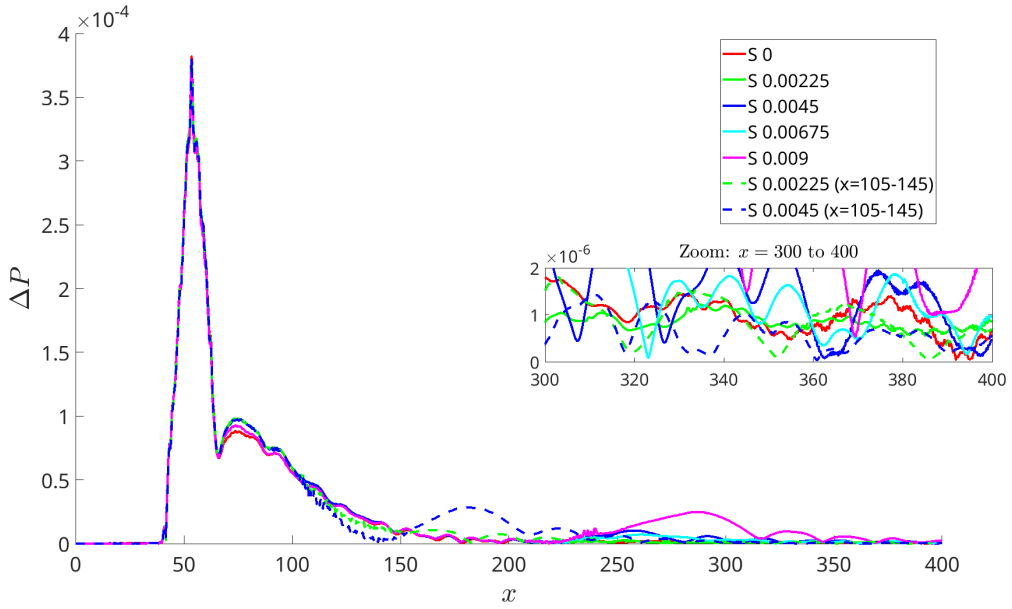

Fig. 14 Streamwise evolution of β = 2 pressure mode amplitude (F = 0.009)

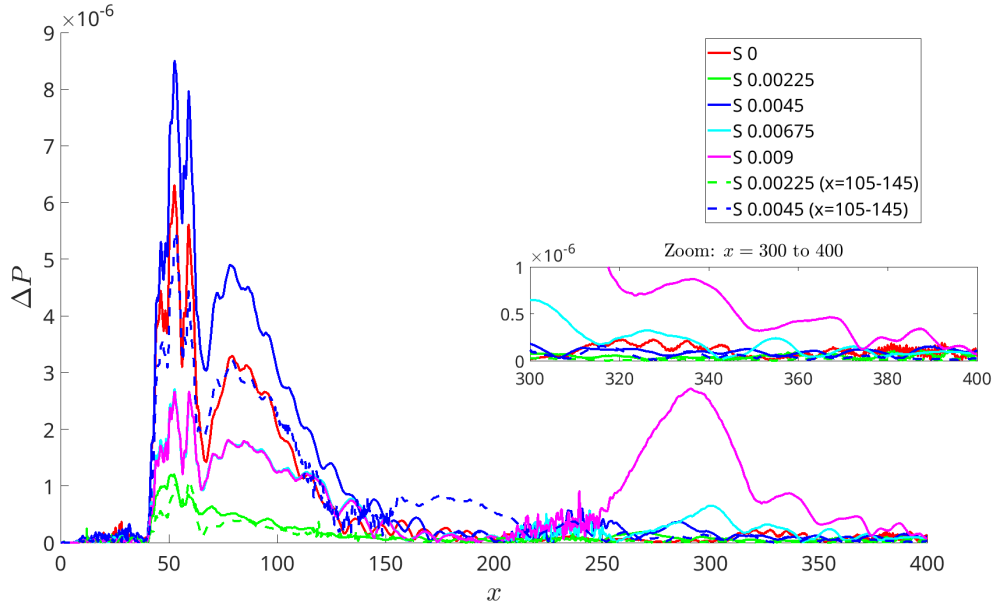

Fig. 15 Streamwise evolution of β = 3 pressure mode amplitude (F = 0.009)

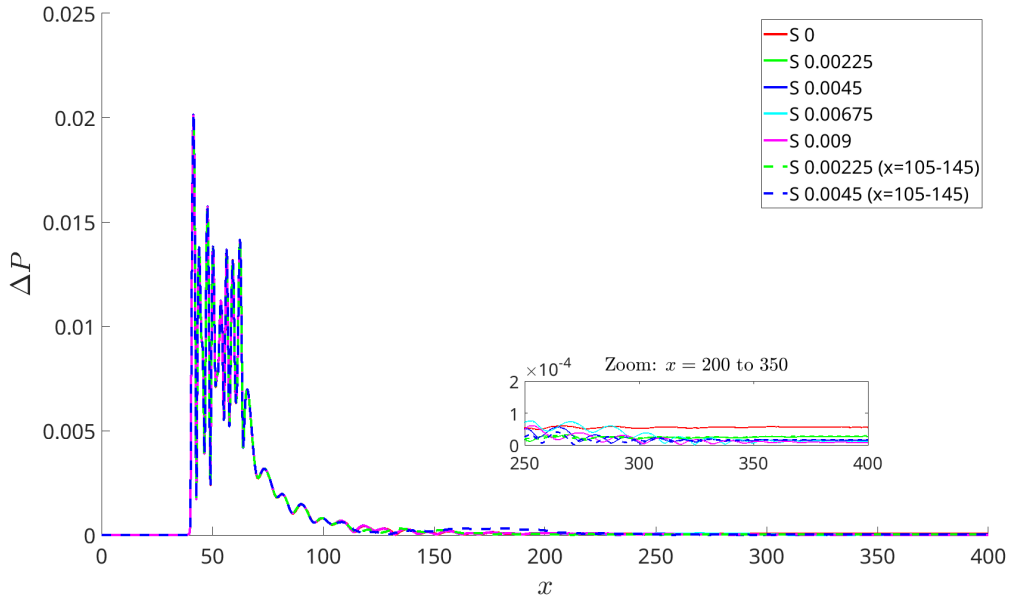

Fig. 16 Streamwise evolution of β = 4 pressure mode amplitude (F = 0.009)

3. Effect on Coolant Retention and Coolant Effectiveness

Cooling Effectiveness has been calculated using Equation 8 in accordance with Keller et al[34].

$$\eta = 1 - \frac{q_c}{q_{wc}} \tag{8}$$

where q_c and q_{wc} depict the heat flux at the wall with and without coolant injection respectively.

Figures 17 and 18 show the near-wall coolant concentration and corresponding cooling effectiveness, respectively. Strong suction draws a significant amount of coolant away from the surface, leading to reduced concentration downstream

and diminished wall cooling. Moderate suction leads to more limited coolant extraction and maintains a higher level of cooling efficiency downstream.

Placing the suction patch immediately downstream of the highest amplitude of disturbances in the no blowing case, between $x = 105$ and $x = 145$, also results in the early local reduction of near-wall coolant. As seen in Figures 17 and 18, early suction reduces the coolant concentration close to the wall very early. However, as seen in Figure 18, the cooling effectiveness curve levels out to a point which appears to be higher than that of the downstream suction cases. When compared downstream, between $x = 200$ and $x = 400$, it is visible that early suction removes the most coolant, followed by the strong suction case applied between $x = 200$ and $x = 240$.

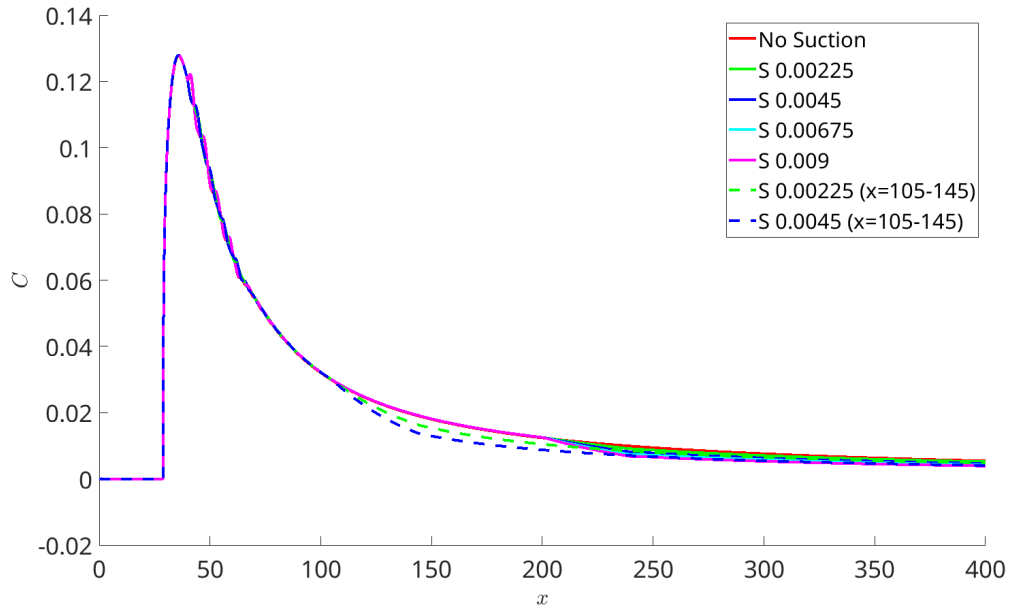

Fig. 17 Near-wall coolant concentration (F = 0.009) for different suction strengths and locations.

The contour plots in Figure 20 illustrate the spatial distribution of coolant mass fraction across the boundary layer for different suction configurations, plotted on the XY plane at mid-span. In the baseline case (S = 0), the injected coolant forms a distinct near-wall layer that gradually spreads downstream, but remains confined close to the wall due to limited mixing, resulting in a high level of coolant close to the wall as seen in Figure 17. As the suction ratio increases, this coolant layer becomes noticeably thinner and more uniform, indicating enhanced near-wall extraction of the coolant and hence reduced vertical penetration into the freestream.

Figure 19 and 20 depict the coolant mass fraction at the wall(top view - XZ plane) and the mid span coolant mass fraction variation(front view - XY plane), respectively. 20f and 20g show that the coolant layer becomes noticeably thin due to early extraction of the coolant. However it can also be noted that the concentration of coolant at the wall appears to be high for a more sustained period of time as visible in Figures 17 and 19f. In the highest suction case (S = 0.009), while the suppression of disturbance growth is most effective, a visible portion of the injected coolant is also extracted from the flow. This highlights a trade-off between maintaining cooling effectiveness and achieving boundary layer stabilization, with excessive suction potentially reducing the net protective benefit of the injected coolant. These results prove that the early suction can result in early removal of the coolant. However, as seen in Figure 18, these configurations prove effective in maintaining a more uniform layer of coolant close to the wall, albeit in lower concentration while late suction allows for a higher concentration of coolant close to the wall, but for a shorter streamwise distance. Therefore, there must exist a balance between the position and the strength of the coolant patch in order to achieve optimal cooling performance.

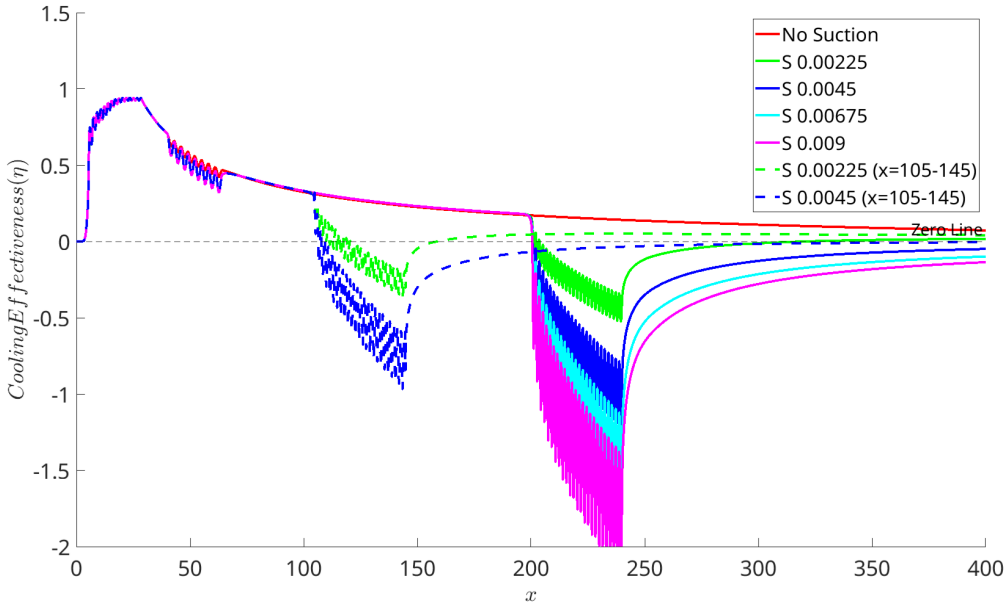

Fig. 18 Wall cooling effectiveness (F = 0.009) as a function of streamwise location

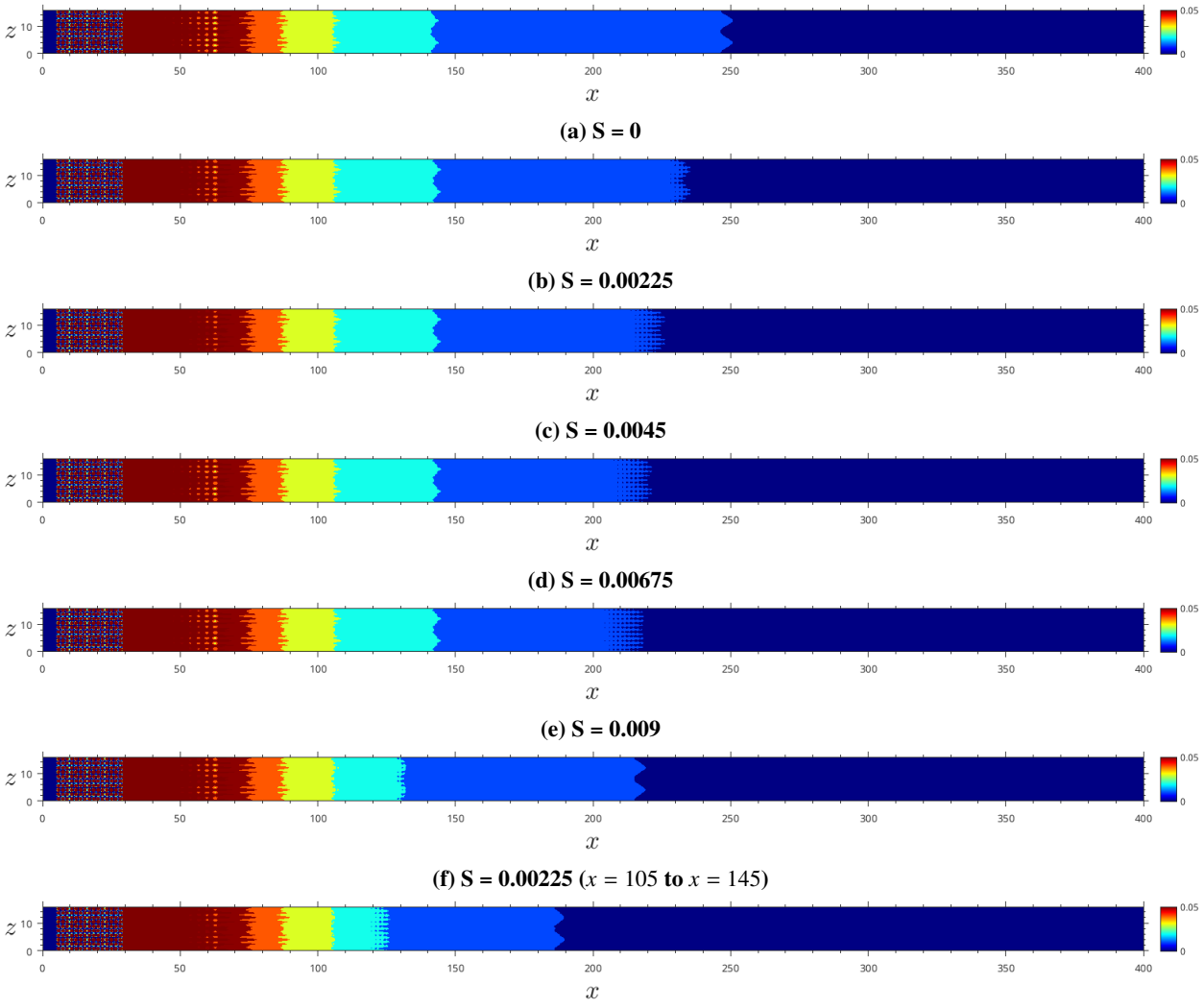

(a) S = 0

(b) S = 0.00225

(c) S = 0.0045

(d) S = 0.00675

(e) S = 0.009

(f) S = 0.00225 (x = 105 **to** x = 145)

(g) S = 0.0045 (x = 105 **to** x = 145)

Fig. 19 Coolant mass fraction contours for various suction ratios at wall (Wall-parallel: XZ Plane)

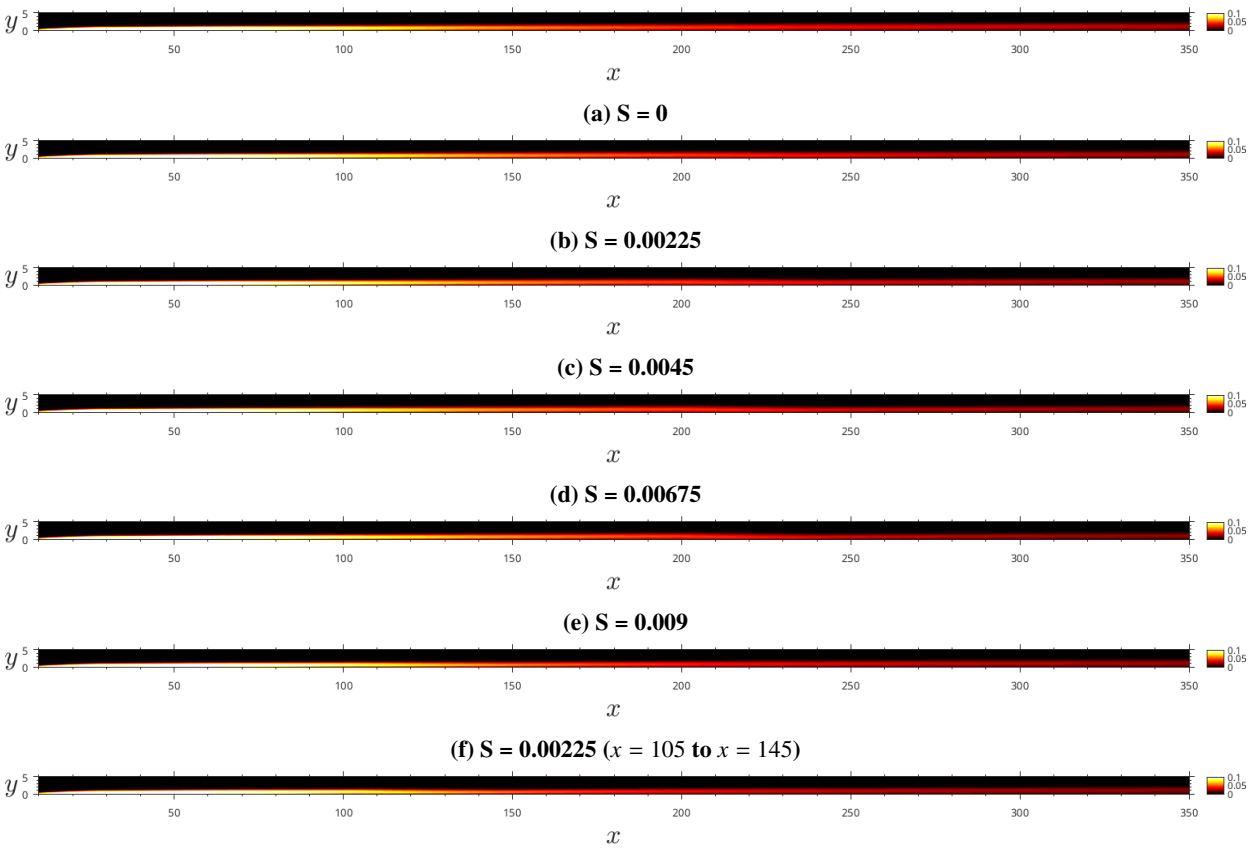

(a) S = 0

(b) S = 0.00225

(c) S = 0.0045

(d) S = 0.00675

(e) S = 0.009

(f) S = 0.00225 (x = 105 **to** x = 145)

(g) S = 0.0045 (x = 105 **to** x = 145)

Fig. 20 Midspan Coolant mass fraction contours for various suction ratios (Wall-normal: XY Plane)

V. Conclusion

The present study investigated the role of localized wall suction on the thermal performance of a transpiration cooling configuration and the receptivity characteristics of a hypersonic boundary layer. DNS simulations were performed with and without coolant injection, with wall-imposed disturbances at different spanwise wavenumbers, and with suction applied at different streamwise locations, namely immediately downstream of the disturbance strip (between x = 105 and x = 145) and further downstream (between x = 200 and x = 240) at multiple suction rates. Disturbance evolution was analyzed via modal decomposition of wall pressure fluctuations, and the impact on coolant retention and cooling performance was evaluated through profiles of near-wall coolant concentration and cooling effectiveness.

For the no-injection($F = 0$) configuration, the absence of coolant allows the effect of pure suction to be observed. It is observed that suction introduces disturbances immediately downstream of the suction patch, which leads to an amplification in the downstream region of wave modes that are seen to decay in the absence of suction, particularly for a 2D mode(β_0) and higher-wavenumber oblique modes, namely the β_3 and β_4 modes. This is representative of the boundary layer receptivity to suction. However, an analysis of the generalized inflection points (GIP) found that suction can locally suppress inflectional behaviour of the boundary layer.

When blowing is introduced (F = 0.009), suction shows a damping effect on specific wave modes, which are otherwise observed to grow rapidly downstream without suction. Suction patches appear to be very efficient in damping the β_0 and β_1 modes which are the primary modes of instability in the boundary layer. The dominant forced mode (β_4) is rapidly attenuated, and other oblique modes are significantly suppressed without signs of downstream re-amplification. However, strong suction is observed to significantly reduce near-wall coolant concentration, leading to diminished surface cooling effectiveness. Early low strength suction placement appears to mitigate this issue, keeping the levels of coolant effectiveness near those seen for the case without suction at larger distances downstream, whilst efficiently damping the disturbances. Conversely, low suction placed downstream appears to provide the highest cooling effectiveness of all the

suction cases by allowing high coolant concentration. This trade-off between strength and position of the suction patch is strongly dependent on the strength of coolant injection, which appears to dictate the damping ability of the suction patch. This balance is very essential to the cooling effectiveness of the cooling mechanism.

In summary, the effectiveness of wall suction depends critically on the upstream flow condition, suction strength, and streamwise location. While suction can suppress instabilities and enhance boundary layer stability, it may play a detrimental effect on the wall-cooling performance. However, a calibration of the suction rate and location of the suction patches can lead to optimized results in terms of both boundary-layer stabilization and high levels of cooling effectiveness. These results indicate the need for integrated aerodynamic and cooling optimization when designing suction-based flow control methods for hypersonic vehicles.

VI. Acknowledgments

The authors would like to acknowledge Sheffield Hallam University for providing the resources necessary for this research. Additionally, the authors would like to thank Engineering and Physical Science Research Council (EPSRC) for the computational time made available on the UK supercomputing facility ARCHER2 via the UK Turbulence Consortium (EP/X035484/1). The author would also like to acknowledge the use of AI in the form of ChatGPT as a tool to conduct spell checks and grammar checks in the paper.

References

[1] Smith, C. R., "Aerodynamic Heating in Hypersonic Flows," *Physics Today*, Vol. 74, No. 11, 2021, pp. 66–67. https://doi.org/10.1063/PT.3.4888.

[2] Sharma, P. K., Deiterding, R., Cerminara, A., and Sandham, N., "Numerical Simulation of Transpiration Cooling for a High-Speed Boundary Layer Undergoing Transition to Turbulence," *Aerospace Science and Technology*, Vol. 141, No. 108581, 2023. https://doi.org/10.1016/j.ast.2023.108581.

[3] Gulhan, A., and Braun, S., "An Experimental Study on the Efficiency of Transpiration Cooling in Laminar and Turbulent Hypersonic Flows," *Experimental Fluids*, Vol. 50, 2011. https://doi.org/10.1007/s00348-010-0945-6.

[4] Ifti, H. S., Hermann, T., Rocher, M., Doherty, L., Hambidge, C., McGilvray, M., and Vandeperre, L., "Laminar Transpiration Cooling Experiments in Hypersonic Flow," *Experiments in Fluids*, Vol. 63, 2022. https://doi.org/10.1007/s00348-022-03446-1.

[5] Naved, I., Hermann, T., Hambidge, C., Ifti, H. S., Falsetti, C., Gianella, S., McGilvray, M., Tirichenko, I. S., and Vandeperre, L., "Transpiration Cooling Heat Transfer Experiments in Laminar and Turbulent Hypersonic Flows," *Journal of Thermophysics and Heat Transfer*, Vol. 37, 2022. https://doi.org/10.2514/1.T6626.

[6] Mi, Q., Yi, S. H., Gang, D. D., Lu, X. G., and Liu, L., "Research Progress of Transpiration Cooling for Aircraft Thermal Protection," *Applied Thermal Engineering*, Vol. 236, 2024. https://doi.org/10.1016/j.applthermaleng.2023.121360.

[7] Liu, X., Bian, Y., Zhou, W., Zhao, X., Jia, Z., and Zhang, Z., "Investigation on the Effectiveness of Transpiration Cooling Under the Influence of Shock Wave," *Applied Thermal Engineering*, Vol. 236, 2024. https://doi.org/10.1016/j.applthermaleng.2023.121831.

[8] Cerminara, A., "Turbulence Effect on Transpiration Cooling Effectiveness Over a Flat Plate in Hypersonic Flow and Sensitivity to Injection Parameters," *Flow, Turbulence and Combustion*, Vol. 110, 2023, pp. 9945–9968.

[9] Heufer, K. A., and Olivier, H., "Experimental and Numerical Study of Cooling Gas Injection in Laminar Supersonic Flow," *AIAA Journal*, Vol. 46, No. 11, 2008. https://doi.org/10.2514/1.34218.

[10] Saric, W. S., Reed, H. L., and Kerschen, E. J., "Boundary-Layer Receptivity to Freestream Disturbances," *Annual Review of Fluid Mechanics*, Vol. 34, No. 1, 2002, pp. 291–319. https://doi.org/10.1146/annurev.fluid.34.082701.161921.

[11] Fedorov, A. V., and Khokhlov, A. P., "Prehistory of Instability in a Hypersonic Boundary Layer," *Theoretical and Computational Fluid Dynamics*, Vol. 14, 2001. https://doi.org/10.1007/s001620100038.

[12] Balakumar, P., "Receptivity of a Supersonic Boundary Layer to Acoustic Disturbances," *AIAA Journal*, Vol. 47, 2009. https://doi.org/10.2514/1.33395.

[13] Ma, Y., and Zhong, X., "Receptivity of a supersonic boundary layer over a flat plate. Part 1. Wave structures and interactions," *Journal of Fluid Mechanics*, Vol. 488, 2003, pp. 31–78. https://doi.org/10.1017/S0022112003004786.

[14] Hader, C., and Laurence, S. J., "Experimental and numerical investigation of second-mode instability growth in a hypersonic boundary layer," *Journal of Fluid Mechanics*, Vol. 804, 2016, p. R1.

[15] Fedorov, A. V., and Khokhlov, A. P., "Receptivity of high-speed boundary layers: mechanisms and methods," *Annual Review of Fluid Mechanics*, Vol. 33, 2001, pp. 341–372.

[16] Esser, B., Barcena, J., Kuhn, M., Okan, A., Haynes, L., Gianella, S., Ortona, A., Liedtke, V., Francesconi, D., and Tanno, H., "Innovative Thermal Management Concepts and Material Solutions for Future Space Vehicles," *Journal of Spacecraft and Rockets*, Vol. 53, 2016. https://doi.org/10.2514/1.A33501.

[17] Tanno, H., "Innovative Thermal Management Concepts for Thermal Protection of Future Space Vehicles - Validation Test Results from Shock Tunnel Facility," Tech. rep., JAXA, 2016.

[18] Cerminara, A., Nayak, R., Potts, J., Tanno, H., Kloker, M. J., Saikia, B., Brehm, C., Camillo, G. P., and Wagner, A., "Transpiration Cooling in Hypersonic Flow and Mutual Effect on Turbulent Transition and Cooling Performance," *Physics of Fluids*, Vol. 37, 2025. https://doi.org/10.1063/5.0253164.

[19] Unnikrishnan, S., and Gaitonde, D. V., "Instabilities and transition in cooled-wall hypersonic boundary layers," *Journal of Fluid Mechanics*, Vol. 915, 2021, p. A26. https://doi.org/10.1017/jfm.2021.84.

[20] Guo, P., Hao, J., and Wen, C. Y., "Interaction and Breakdown Induced by Multiple Optimal Disturbances in Hypersonic Boundary Layer," *Journal of Fluid Mechanics*, Vol. 974, 2023. https://doi.org/10.1017/jfm.2023.814.

[21] Unnikrishnan, S., and Gaitonde, D. V., "Linear, Nonlinear and Transitional Regimes of Second-Mode Instability," *Journal of Fluid Mechanics*, Vol. 905, 2020. https://doi.org/10.1017/jfm.2020.781.

[22] Egorov, I. V., Fedorov, A. V., and Soudakov, V. G., "Disturbances generated by suction–blowing in a hypersonic boundary layer," *Theoretical and Computational Fluid Dynamics*, Vol. 20, 2006, pp. 41–54. https://doi.org/10.1007/s00162-005-0001-y.

[23] Zhuang, G. H., Wan, Z. H., Liu, N. S., Sun, D. J., and Lu, X. Y., "Instability and Transition Control by Steady Local Blowing/Suction in a Hypersonic Boundary Layer," *Journal of Fluid Mechanics*, Vol. 990, 2024. https://doi.org/10.1017/jfm.2024.539.

[24] Keller, M. A., and Kloker, M. J., "Direct Numerical Simulation of Foreign-Gas Film Cooling in Supersonic Boundary Layer Flow," *AIAA Journal*, Vol. 55, 2017. https://doi.org/10.2514/1.J055115.

[25] Carpenter, M. H., Nordstrom, J., and Gottlieb, D., "A Stable and Conservative Interface Treatment of Arbitrary Spatial Accuracy," *Journal of Computational Physics*, Vol. 148, No. 2, 1999. https://doi.org/10.1006/jcph.1998.6114.

[26] Ducros, F., Ferrand, V., Nicoud, F., Weber, C., Darracq, D., Gacherieu, C., and Poinsot, T., "Large-Eddy Simulation of the Shock/Turbulence Interaction," *Journal of Computational Physics*, Vol. 152, No. 2, 1999. https://doi.org/10.1006/jcph.1999.6238.

[27] Yee, H. C., Sandham, N. D., and Djomehri, M. J., "Low-Dissipative High-Order Shock-Capturing Methods Using Characteristic-Based Filters," *Journal of Computational Physics*, Vol. 150, No. 1, 1999. https://doi.org/10.1006/jcph.1998.6177.

[28] Sandham, N. D., Li, Q., and Yee, H. C., "Entropy Splitting for High-Order Numerical Simulation of Compressible Turbulence," *Journal of Computational Physics*, Vol. 178, No. 2, 2002. https://doi.org/10.1006/jcph.2002.7022.

[29] De Tullio, N., Paredes, P., Sandham, N. D., and Theofilis, V., "Laminar–Turbulent Transition Induced by a Discrete Roughness Element in a Supersonic Boundary Layer," *Journal of Fluid Mechanics*, Vol. 735, 2013. https://doi.org/10.1017/jfm.2013.520.

[30] Cerminara, A., "Boundary-Layer Receptivity and Breakdown Mechanisms for Hypersonic Flow Over Blunt Leading Edge Configurations," Ph.D. thesis, University of Southampton, 2017.

[31] Balakumar, P., "Receptivity of Hypersonic Boundary Layers to Acoustic and Vortical Disturbances," *45th AIAA Aviation Forum*, 2015. https://doi.org/10.2514/6.2015-2473.

[32] Wang, X., Zhong, X., and Ma, Y., "Response of a hypersonic boundary layer to wall blowing–suction," *AIAA Journal*, Vol. 49, No. 7, 2011, pp. 1336–1353. https://doi.org/10.2514/1.J050173.

[33] Fedorov, A. V., Egorov, I. V., and Soudakov, V. G., "Receptivity of a hypersonic boundary layer over a flat plate with a porous coating," *Journal of Fluid Mechanics*, Vol. 601, 2008, pp. 165–187. https://doi.org/10.1017/S0022112008000669.

[34] Keller, M. A., Kloker, M., and Olivier, H., "Influence of Cooling-Gas Properties on Film-Cooling Effectiveness in Supersonic Flow," *Journal of Spacecraft and Rockets*, Vol. 52, 2015. https://doi.org/10.2514/1.A33203.